Dissertation

Atomic and electronic structures of group IV-VI two dimensional materials
(IV-VI 族２次元物質の原子及び電子構造)

Graduate School of
Natural Science & Technology
Kanazawa University

Division of Mathematical and
Physical Sciences
Kanazawa University

Student ID No: 1824012001
Name : Aflah Zaharo
Chief Advisor: Prof. Mineo Saito

12 January 2022

List of publication:

1. A. Zaharo, A. Purqon, T. Winata and M. Saito, Electronic structure of puckered grup -IV-VI two dimensional monolayers materials, Japanese Journal of Applied Physics, 59, 071006, June 2020.

Atomic and electronic structures of group IV-VI two dimensional materials

(IV-VI 族 2 次元物質の原子及び電子構造)

Aflah Zaharo

Abstract

Two-dimensional materials have attracted scientific interest because of their novel electronic properties. Successfully phosphorene from black-phosphorus shows potential application on optoelectronic devices due to its moderate bandgap and the properties of another 2D materials in group IV-VI. In this research, we carry out first-principles calculations on monolayer group IV-VI 2D materials. We study systems consisting of group IV elements (C, Si, Ge) and group VI elements (O, S, Se, Te) and find that all the materials form buckled puckered geometries. We clarify that VI atoms tend to be located at the lower positions in the buckled structure when the electronegativity of the VI atom is sufficiently larger than that of the IV atom, which is due to the electron transfer from the IV atom to the VI atom. We find that all the calculated bands are doubly degenerated on the first Brillouin zone edge due to the symmetry of this system. The degeneracies originate from pairing of conventional one-dimensional irreducible representation or from nonconventional two-dimensional irreducible representation.

Keywords: Two-dimensional materials, IV-VI materials, density functional theory, first-principles calculation, band structure, group theory.

Acknowledgements

I would like to express my sincere gratitude to my Supervisor, Professor Mineo Saitou, for the continuous support of my Master study and research, for his patience, motivation, and immense knowledge. His guidance helped me in all time of research and writing my dissertation.

My sincere thank also goes to my family, father, mother, sister, and brother in Indonesia. Because of their pray and support, I can struggle and fulfill of motivation when I am studying here. I want to thank my laboratory mate, Yusuf-san, Rifki-san, Monika-san, Manaf-san and Minami-san for the kind and warmly discussion. Last but not least, my sincere thank goes to Kanazawa University, who have given me a chance to study in Japan.

Contents

List of Figures

List of Tables

Chapter 1

Introduction

1.1 Background and Motivation

Two-dimensional materials have been stimulating scientific and technological interests because of their novel electronic properties. At first, two-dimensional material was assumed to be thermodynamically unstable due to small thickness [1]. However, in 2004, the discovery of graphene opened the gateway into the field of group IV based 2D monolayer materials [1, 2]. K. S. Novoselov and and A. K Geim have successfully discovered graphene through mechanical exfoliation and it shows high electronic quality [2][3]. The small size of the material has lets to the strong interatomic bond that ensure the thermal stability [4]. Following discovery of graphene, analogues of graphene in group IV compounds have been produced such as silicene, [3-5], germanene [6] and stanene [7]. In particular, the Dirac cone in the electronic band structures characterizes the electronic properties of group IV materials [8, 9].

However, the absent of band gap in 2D group-IV materials have limits their application in several electronic devices. Therefore, researchers try to find 2D materials with finite band gap. In 2014, phosphorene was successfully synthesized from black phosphorus [10-12]. In sharp contrast to group IV 2D materials, it was found that phosphorene has a moderate band gap and is suitable for field-effect transistor material [13-15]. Its bandgap is larger than that of the black phosphorus bulk and decreases as the layer becomes thick, which was first discovered based on a first-principles calculation [16]. Phosphorene also shows high hole mobility compared to the graphene (above 10000 cm^2/Vs). As well as phosphorene, other group V materials have been studied such as arsenene [17-20], antimonene [21-23] and bismuthene [24-27]. The previous calculation showed that the energy difference between the puckered and six-member-ring structures is small [17, 28]

and they are candidates for optical device and thermoelectric materials [29]. All these properties also show high holds a great potential for future applications and therefore it motivates researchers to find another possible 2D monolayer materials in group-V compounds.

Recently, IV-VI 2D systems attractive scientific and technological attentions [30, 31]. The advantages of 2D group IV–VI compounds, such as unique orthorhombic structures, environmentally friendly features, being earth-abundant and low-cost further improve their properties and deepen their applications into a broader space. The monolayers form structures belonging to the same orthorhombic crystal system, and possess similar hinge-like structure like phosphorene, which is a typical feature distinctly different to flat graphene and buckled silicene. Just this unique hinge-like structure and the isolation of 2D forms will introduce strong anisotropic properties, making the group IV–VI compound monolayers very attractive for large-scale applications in photovoltaics and thermoelectric. The previous calculation showed the puckered structures are more stable than the six-member-ring one in most of the cases and monolayer systems are candidates for optical device materials [32-35]. Therefore, clarification of their electronic structures is necessary.

1.2 Research Objective

We in particular focus on electronic band structures of the first Brillouin zone edge IV atoms and group VI atoms monolayers with group IV consist of C, Si, Ge and group VI consist of O, S, Se, Te by employing density functional theory (DFT). This choice of elements would give ten possible combinations of materials, namely CSe, CTe, SiO, SiS, SiSe, SiTe, GeO, GeS, GeSe and GeTe. The properties of the binary 2D systems can be entirely different from those of elemental 2D systems. In this paper, we systematically study the electronic and atomic structures of the buckled puckered structures of group IV-VI two-dimensional monolayers materials. We perform first-principles density-functional based calculations. We first optimize the geometries of buckled-puckered

structures of monolayer group IV-VI two-dimensional materials. Next, we clarify the relation between buckling height and electron transfer of buckled-puckered structures of monolayer group IV-VI two-dimensional materials. In the last we calculate the band structures and analyze them based on the group theory.

1.3 Outline of Dissertation

This dissertation consists of six chapters. Chapter 1 gives the background of the research. Chapter 2 introduces the theoretical background of density functional theory (DFT) and group theory analysis to identify the irreducible representations of band structure. Chapter 3 will perform he theoretical background of group theory to understand the irreducible on the several band structure at some k-point of first Brillouin zone. Chapter 4 presents the results calculation electronic structure of monolayer puckered group IV-VI materials. First, we clarify the relation between the buckling amplitudes and the electrons transfer between the IV and VI atoms. Next, we analyze the degeneracy on first Brillouin zonw edge of the band structures based on the group theory. Chapter 5 summarizes the results and present the future scopes that can be considered from this research.

Chapter 2

Theoretical Background

The method of this research is the simulation based on the Density Functional Theory (DFT). DFT is one of quantum mechanical approaches to describe matter. The main idea of DFT is to describe the interacting electron system in the form of electronic density [36]. In this chapter, we describe the theory of this thesis. We present the basic of density functional theory for electronic calculation in section 2.1. In the section 2.2 and 2.3 we explained the reason of the degeneracy on the first Brillouin zone based on the group theory. Next, we explain the application of DFT in Section 2.4.

2.1 Hohenberg-Kohn Theorem

The idea of DFT is based on the theory from Hohenberg and Kohn [37]. This theorem justified that the electron density is the central quantity to find the information of electronic properties.

Theorem 1. The ground state energy from Schrödinger's equation is a unique functional of electron density.

The important thing of this theorem is we must know about the meaning of functional. Here, we can say that the functional is a function of a function. The theorem states that there exists a one-to-one mapping between the ground-state wave function and the ground-state electron density. So, we can say that the ground state E can be represented by $E[n(r)]$ where $n(r)$ is the electron density. The electron density of n electrons, is defined by using the wave function, which is expressed as:

$$\mathrm{n(r)} = \sum_{i=1}^{N} \int \dots \int d_{r1} d_{rN} \psi * (r_1, \dots, r_N) \xi (r_1 - r) \psi (r_1, \dots, r_N) \quad (2.1)$$

From (2.1), we can conclude that the energy can be written as a functional of electron density but not the wave function.

Theorem 2. The electron density that minimizes the energy of the overall functional is the true electron density corresponding to the full solution of the Schrödinger equation.

The second theorem states that the total energy functional is expressed by:

$$E_{HK}[n] = T[n] + E_{int}[n] + \int V_{ext}(r) n(r) dr + E_N \quad (2.2)$$

$E_{HK}[n]$ is total energy functional, $T[n]$ is kinetic energy, $E_{int}[n]$ is the energy of electron's interaction, and E_N is the energy of nuclei - nuclei interaction (it is independent to density).

2.2 The Kohn-Sham Equation

The Kohn-Sham equation approach is based on replacing electron interaction by using the non-interacting electrons, which is under an effective potential [37]. Kohn and Sham suggested that the true electron density will minimize the total energy by calculating from a system of non-interacting electrons moving in the effective potential [37]. The ground state charge density for a system with non-interaction electron can be defined as

$$n(r) = 2 \sum_{i}^{N} |\psi(r)|^2 \quad (2.3)$$

The electron density $n(r)$ can be changed by changing the $\psi(r)$. The effective potential consists of the external potential, the Coloumb interaction between electrons, and the exchange-correlation interactions. So the energy functional can

be expressed by:

$$E_{KS}[n(r)] = T[s][n(r)] + E_H[n(r)] + E_{XC}[n(r)] + \int V_{ext} n(r) dr \quad (2.4)$$

$T[s][n(r)]$ is the kinetic energy of non-interacting electrons. It can be expressed by:

$$T[s][n(r)] = -\int \psi_i^*(r) \nabla^2 \psi_i(r) dr \quad (2.5)$$

$E_H[n(r)]$ is the Hartree energy which defined as

$$E_H[n(r)] = \frac{1}{2} \int \frac{n(rn(r'))}{r - r'} dr dr' \quad (2.6)$$

$+E_{XC}[n(r)]$ is the exchange and correlation energy terms, when all of the functional $+E_{XC}[n(r)]$is known, so the exact ground state density and the energy of the many body problem can be found.

Because of the fact that Kohn-Sham energy is minimization problem with respect to the density, the derivation of (2.2) can be expressed by

$$\frac{\delta E_{KS}}{\delta \psi_i^*(r)} = \frac{\delta T}{\delta \psi_i^*(r)} + \left[\frac{\delta E_{ext}}{\delta n(r)} + \frac{\delta E_H}{\delta n(r)} + \frac{\delta E_{XC}}{\delta n(r)}\right] \frac{\delta n(r)}{\delta \psi_i^*(r)} - \frac{\delta(\lambda(\int n(r) dr - N))}{\delta n(r)} \left[\frac{\delta n(r)}{\delta \psi_i^*(r)}\right] = 0 \quad (2.7)$$

by setting that

$$\frac{\delta n(r)}{\delta \psi_i^*(r)} = 2 \quad (2.8)$$

each term of (2.7) can be written as

$$\frac{\delta T}{\delta \psi_i^*(r)} = -\nabla^2 \psi_i(r), \quad (2.9)$$

$$\left[\frac{\delta E_{ext}}{\delta n(r)}+\frac{\delta E_H}{\delta n(r)}+\frac{\delta E_{XC}}{\delta n(r)}\right]\frac{\delta n(r)}{\delta \psi_i^*(r)}=2(V_{ext}+V_H+V_{XC})\psi_i(r) \quad (2.10)$$

$$\frac{\delta(\lambda(\int n(r)dr-N))}{\delta n(r)}\left[\frac{\delta n(r)}{\delta \psi_i^*(r)}\right]=2\in_i \psi_i(r) \quad (2.12)$$

Then, we can insert (2.9), (2.10), and (2.11) to (2.7) then get the Kohn-Sham equation as:

$$\left[-\frac{1}{2}\nabla^2+V_{KS}(r)\psi_i(r)=\in_i \psi_i(r)\right] \quad (2.12)$$

where

$$V_{KS}(r)=V_{ext}(r)+V_H(r)+V_{XC}(r)$$

$$=V_{ext}(r)+\frac{1}{2}\int\frac{n(r')}{r-r'}dr'+V_{XC}(r) \quad (2.13)$$

The many-electrons problem becomes to one electron problem when the virtual independent-particle system has the same ground state as the real interacting system. So it can be defined as

$$V_{KS}(r)=V_{eff}(r) \quad (2.14)$$

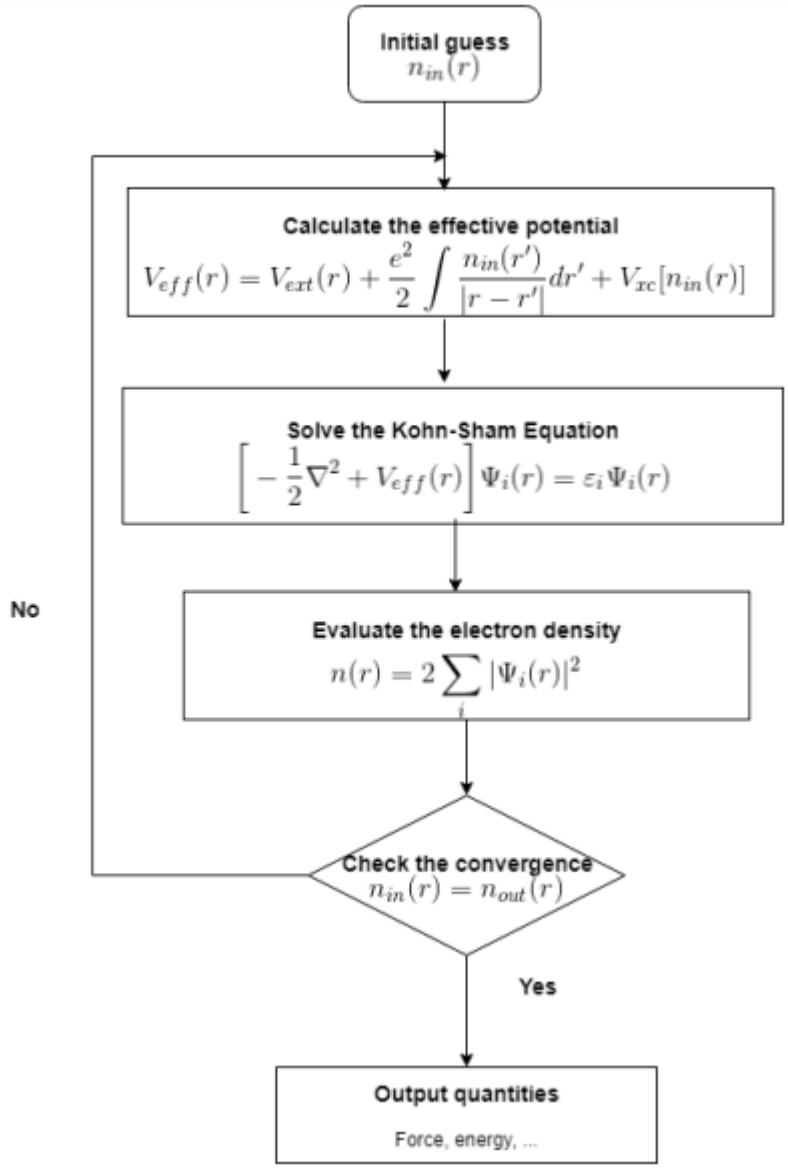

Fig. 2.1 Self-consistent loop for Kohn-Sham equation's solution

And then, the kinetic energy can be written as

$$T[s][n(r)] = \sum_i \in_i - \int n(r)V_{eff}\, r(dr) \tag{2.15}$$

So, the total energy of Kohn-Sham equation is

$$E_{KS}[n(r)] = \sum_i + \frac{1}{2}\int\int \frac{n(r)n(r')}{r-r'}drdr' + E_{XC}[n(r)]$$
$$- \int n(r)V_{eff}(r)dr \quad (2.16)$$

Both E_{XC} and V_H depend on $n(r)$, it means that they also depend on $\psi_i(r)$. By using the self-consistent method as shown at flowchart in Fig.2.1, the Kohn-Sham equation can be obtained. An initial guess of $n(r)$ is defined first, then calculates the V_H and V_{XC} to get V_{KS}. By solving the Kohn-Sham equation, the ψ_i can be obtain and we get new density (which is obtained by the result of ψ_i). The new density then can be used as the new guess $n(r)$ and used to calculate the new V_{KS}. It repeated until we get the convergence result.

2.3 Exchange Correlation Function

In a realistic condensed matter-system frame, it is necessary to find an accurate exchange correlation energy functional $E_{XC}[n(r)]$. In the case of homogeneous electronic system, the E_{XC}only depends on the density. But in the case of non-homogeneous electronic system, the functional of $E_{XC[nr]}$. at point r also depend on the variation at near r point.

2.3.1 Local Density Approximation (LDA)

Hohenberg and Kohn suggested a simple approximation called LDA or in the spin polaraized case the local-spin-density approximation (LSDA). The exchange-correlation energy per particle by its HEG (homogeneous electron gas) $e_{xc}[n(r)]$ is expressed by

$$E_{XC}^{LDA}[n(r)] = \int n(r)e_{xc}^{homo}(n(r))dr$$
$$= \int n(r)\left[e_X^{homo}\left(n(r)\right) + e_C^{homo}n(r))\right]dr \quad (2.17)$$

for the spin polarized system

$$E_{XC}^{LDA}[n_+(r), n_-(r)] = \int n(r) e_{xc}^{homo}(n_+(r), n_-(r))dr \tag{2.18}$$

where the exchange energy $e_x(n(r))$ given by

$$e_x\big(n(r)\big) = -\frac{3}{4\pi}k_f \tag{2.19}$$

where $k_f$is the Fermi wave vector $k_f = (3\pi^2 n)^{\frac{1}{3}}$. The correlation energy density of HEG at high density limit has the form

$$e_c = Aln(r_s) + B + (r_s)(Cln(r_s) + D) \tag{2.20}$$

and the density limit

$$e_c = \frac{1}{2}\left(\frac{g_0}{r_s} + \frac{g_0}{r_{s^{\frac{3}{2}}}} + \cdots\right) \tag{2.21}$$

r_s is the Wigner-Seitz radius r_s is related to the density as

$$r_s = \left[\frac{3}{4\pi n}\right]^{\frac{1}{3}} \tag{2.22}$$

At the spin-polarized system, the exchange energy functional is known exactly from the result of spin-unpolarized functional

$$E_X[n_+(r), n_-(r)] = \frac{1}{2}(E_X[2n + (r)] + E_X[2n - (r)]) \tag{2.23}$$

The spin-dependence of the correlation energy density is approached by the relative spin-polarization

$$\varepsilon(r) = \frac{n_+(r) - n_-(r)}{n_+(r) + n(r)} \tag{2.24}$$

The spin correlation energy density $e_c(n(r), \varepsilon(r))$ is constructed to interpolate extreme value $\varepsilon = 0, \pm 1$, corresponding to spin-unpolarized and ferromagnetic situation. The xc potential $V_{XC}(n(r))$ in LDA is given by

$$\frac{E_{XC}[n]}{\delta n(r)} = \int dr \left[\epsilon XC + n\frac{\partial \epsilon XC}{\partial n}\right] \tag{2.25}$$

$$V_{XC}(r) = \epsilon_{xc} + n\frac{\partial \epsilon_{xc}}{\partial n} \tag{2.26}$$

$$E_{XC}[n] = \int drn(r)\epsilon_{xc}([n], r) \tag{2.27}$$

where $\epsilon_{xc}([n],)$ is the energy per electron that depends only on density $n(r)$

The LDA has useful predictions of electron densities, atomic positions, and vibration frequencies. But, sometimes LDA also has some errors, for example the total energies of atoms are less realistic than those of HF approximations, and binding energies are overestimated, and then LDA also systematically underestimates the band gap.

2.3.2 Generalized Gradient Approximation (GGA)

In the case of inhomogeneous density, naturally, we have to carry out the expansion of electronic density in the term of gradient and higher order derivatives, and they are usually termed as generalized gradient approximation (GGA). GGAs are still local but also take into account the gradient of the density at the same coordinate. The definition of exchange-correlation energy functional of GGA is the generalized form including the corrections from density gradient $\nabla n(r)$ as:

$$\mathrm{E}_{XC}^{GGA}[n_+(r), n_-(r)]$$
$$= \int n(r)e_x\left[n(r)F_{XC}[n(r)_+, n(r)_{-,}|\nabla \mathrm{n}(r)_+|, |\nabla \mathrm{n}(r)_-|, \ldots\right]dr \tag{2.28}$$

F_{XC} is the escalation factor that modifies the LDA expression according to the variation of density in the vicinity of the considered point, and it is dimensionless [38]. The exchange energy expansion will introduce a term that proportional to the squared gradient of density. If we considered up to fourth order, the similar term also appears proportional to the square of density's Laplacian. Recently, the general derivation of the exchange gradient expansion has been up to sixth order by using second order density response theory [39]. The lowest order (fourth order) terms in the expansion of F_x have been calculated analytically [38, 40]. This term is given by

$$F_X(m,n) = 1 + \frac{10}{81}m + \frac{146}{2025}m^2 - \frac{73}{405}nm + Dm^2 + O\left(\nabla_\rho^6\right) \tag{2.29}$$

where:

$$m = \frac{\left|\nabla_\rho\right|^2}{4(3\pi^2)^{\frac{2}{3}}\rho^{\frac{8}{3}}} \tag{2.30}$$

is the square of the reduced density gradient, and

$$n = \frac{\left|\nabla_\rho\right|^2}{4(3\pi^2)^{\frac{2}{3}}\rho^{\frac{5}{3}}} \tag{2.31}$$

is the reduced Laplacian density

Here some comparation between GGAs and LDA (LSDA):

1. GGA enhances the binding energies and atomic energies.

2. GGA enhances the bond length and bond angles.

3. GGA enhances the energies, geometrics, and dynamical properties of water, ice, and water cluster.

4. Semiconductors are marginally better described within the LDA than GGA,

except for the binding energies.

5. For the 4d - 5d transition metals, the improvement of GGA over LDA is not clear, depends on how well the LDA does in each particular case.

6. Lattice constant of Ag, Au, and Pt are overestimated in GGA.

7. The improvement in the gap energy is obtained, but, it is not substantial as this feature related to the description of the screening of the exchange hole when one electron is removed, at this point is not taken into account by GGA.

2.4 Plane-Wave Basis Set

Plane-waves method centered throughout the complete space not only at the nuclei. The Kohn-Sham equation can be described by using plane waves. As the arrangement of the atoms within the cell is periodic in the real space, so the wave functions must satisfy Bloch's theorem, which can be written by:

$$\psi_i(r) = \exp(ik.r)\, u_k(r) \tag{2.32}$$

$u_k(r)$ is periodic in space with the same periodicity with the cell which can be expanded into a set of plane waves

$$u_i(r) = \sum_G c_{i,G} \exp\,(iG.r) \tag{2.33}$$

We can subtitute (2.33) to (2.32) so the electronic wave function can be expressed as:

$$\psi_i(r) = \sum_G c_{i,k+G} exp\,(i(k+G).r) \tag{2.34}$$

The Kohn-Sham equation became

$$\sum_{G'} \left[\frac{1}{2}|k+G|^2\delta\right] \tag{2.35}$$

The Kohn Sham equation then substituted in terms of reciprocal space r as

$$\sum_{G'}\left[\frac{1}{2}|k+G|^2\delta_{G,G'}+V_{KS}(G'-G)\right]c_{i,k+G}=\epsilon_i c_{i,k+G} \tag{2.36}$$

The Kohn-Sham equation's solution can be reached by diagonalization of the Hamiltonian matrix. The kinetic term is at the diagonal part, otherwise are the potential term. The cut off energy is applied to the kinetic energy term in order to limit the summation over G. It can be expressed as

$$E_{cut}=\frac{1}{2}|k+G|^2 \approxeq G_{cut}^2 \tag{2.37}$$

The limitation of energy is in order to get the lower energy because the lower energy is more important.

2.5 Pseudopotential

The main application of pseudopotential in electronic structure is to replace the strong Cuoloumb potential of the nucleus and the effect of the tightly bound core electrons by an effective ionic potential acting on the valence electrons. Two types of famous pseudopotentials are norm conserving and ultrasoft pseudopotential.

Norm Conserving Pseudopotential

There are some requirements to be fulfilled in this pseudopotential [41]

1. All the electrons and pseudo valence eigenvalues are the same as the selected atomic configuration.

$$\epsilon_i^{AE}=\epsilon_i^{PS} \tag{2.38}$$

2. All the electrons and pseudo valence eigenvalues are in agreement in an external core region.

$$\psi_i^{AE}(r)=\psi_i^{PS}(r), r\geq R_c \tag{2.39}$$

3. The logarithmic derivatives and their first energy derivative of real and pseudo wave functions match at the cut off radius R_c.

$$\frac{d}{dr} ln\psi_i^{AE}(r) = \frac{d}{dr} ln\psi_i^{PS}(r) \tag{2.40}$$

4. The total charge inside core radius RC for each wave function must be same (norm conservation).

$$\int_0^{R_C} dr\left|\psi_i^{AE}(r)\right|^2 = \int_0^{R_C} dr\left|\psi_i^{PS}(r)\right|^2 \tag{2.41}$$

5. The first energy derivative of the logarithmic derivatives of all-electrons and pseudo wave functions must be same for $r \geq R_C$

Ultrasoft Pseudopotential

Vanderbilt obtained the ultrasoft pseudopotential to get the smoother pseudo wave functions, [42]. The pseudo wave functions are divided into two parts:

1. Ultrasoft valence wave functions which omit norm conservation criteria Φ_I^{US}.

2. A core augmentation charge.

$$Q_{nm}(r) = \psi_i^{AE_*}(r)\psi_i^{AE}(r) - \psi_n^{US_*}(r)\psi_m^{US}(r) \tag{2.42}$$

The ultrasoft pseudopotential takes the form of

$$V^{US} = V_{loc}(r) - \sum_{nml} D_{mn}^0 |\beta_n^l\rangle\langle\beta_m^l| \tag{2.43}$$

Where β is the projector function which is expressed by

$$|\beta_n\rangle = \sum_m \frac{|X_m\rangle}{\langle X_m|\phi_n\rangle} \tag{2.44}$$

they are strictly localized inside the cut off region for the wave functions since the X-functions are defined through

$$|X_n\rangle = \left(\epsilon_n - \hat{T} - V_{loc}\right)|\phi_n\rangle \tag{2.45}$$

$$D_{nm}^0 = \quad \langle\phi_n\rangle|X_m\rangle + \epsilon_m q_{nm} \tag{2.45}$$

The scattering properties of the pseudopotential can be improved by using more than one β projector function per angular momentum channel. It is necessary to use the generalized eigen value formalism. For this case we introduce the overlap operator $\hat{S}$

$$\hat{S} = 1 + \sum_{nml} q_{nm}|\beta_n^l\rangle\langle\beta_m^l| \tag{2.47}$$

where

$$q_{nm} = \int_0^{r_c} dr Q_{nm}(r) \tag{2.48}$$

The charge density is expressed by

$$n_r = \sum_i \phi_i^*(r)\hat{S}\phi_i(r)$$

$$= \sum_i |\phi_i(r)|^2 + \sum_{nml} Q_{nm}^I(r)\langle\phi_i|\beta_n^I\rangle\langle\beta_m^I|\phi_i\rangle \tag{2.49}$$

The above-mentioned plane-wave pseudopotential method is implemented in PHASE/0 code [43]. PHASE is a free software developed by the members of the Theory Group of Joint Research Center of Atom Technology (JRCAT) in 1993-2001. Since 2002, the development of this program is leading by Center for Research on Innovative Simulation Software (CISS), the Institute of Industrial Science (IIS), the University of Tokyo. PHASE is a first-principles electronic structure calculation program based on DFT. It means that no experimental results

use to fit the parameter. This program is using plane wave-basis to do the calculation. We can do calculation using pseudopotential or projected augmented wave (PAW). Calculation procedures start with setting of atomic position, wavefunction, and electron density in input file. We can also specify which wavefunction solver we use to update the wavefunction. Then, using wavefunction solver and initial wavefunction, the calculation begins. The whole calculations are finished where the atomic force is lower or same as threshold force.

2.6 Calculation Parameters

The puckered buckled system consists of four atoms, two atoms from group IV and two atoms from group VI. We carry out density functional band structure calculations to obtain the Bloch wavefunctions, $\Psi_k^j(\vec{r})$. We use the exchange-correlation function of the generalized gradient approximation (GGA). [44, 45] The ultrasoft [45] and norm-conserving [46] pseudopotentials are used for carbon, oxygen, and tellurium and for silicon, sulfur, germanium, and selenium atoms, respectively. The cutoff energies of the wavefunctions are 25 (30) Rydberg and charge density is 225 (150) Rydberg for ultrasoft (norm-conserving). We use $15 \times 15 \times 1$ k sampling points in the Brillouin zone integrations and the optimized geometries is under the condition that the atomic forces are less than 0.005 eVÅ−1.

Chapter 3

Group Theoretical Analysis of Band Structures

We analyze the calculated wave functions based on the group theory. In the first section of this chapter, we explain the theoretical background of group theory to understand the irreducible on the several band structure at some *k*-point on first Brillouin zone edge. In second section we discuss the reason of doubly degeneracy on the first Brillouin zone edge.

3.1 Group Theory Representation in Band Structure

The symmetry operation $\hat{R}_i$ is given by:

$$\hat{R}_i = \{\theta_i|\vec{\tau}_i\} \tag{3.1}$$

where θ_i and $\vec{\tau}_i$ represent rotation and fractional translation, respectively.[47] We consider a Bloch wavefunction, $\Psi_k^j(\vec{r})$, given by:

$$\Psi_k^j(\vec{r}) = \frac{1}{\sqrt{NV}} e^{(i\vec{k}\bullet\vec{r})} \sum_n c_j(\vec{G}_n) e^{(i\vec{G}_n\bullet\vec{r})} \tag{3.2}$$

where $\vec{G}_n$ and $\vec{k}$ are a reciprocal lattice vector and a wave vector in the first Brillouin zone, respectively. $c_j(\vec{G}_n)$ is a coefficient and the band index j is in the ascending order of energy. N is the total number of unit cells and V is the volume of each unit cell. The irreducible representations of wavefunctions are determined by evaluating the following expression:

$$Q^\alpha = \frac{1}{l} \sum_i \chi^\alpha(R_i)^* \langle\Psi|\hat{R}_i|\Psi\rangle \tag{3.3}$$

where l and $\chi^{\alpha}(R_i)$ are the order of the group and the character of the irreducible representation of α, respectively, and *i* runs over the symmetry operations of the *k* group. When $Q = 1(Q = 0)$, the wavefunctions belong to (do not belong to) the *l*th irreducible representation. By using Eq. (3.1), Eq. (3.2) is expressed as:

$$Q^{\alpha} = \sum_i \acute{\chi}^{\alpha}(R_i)^* \sum_n c_j(\vec{G}_n)\, c_j\left(\theta_i \vec{G}_n - \vec{G}'\right)^* e^{\left(-i(\theta_i \vec{G}_n - \vec{G}')\bullet\vec{\tau}_i\right)} \tag{3.4}$$

where $\vec{k}$ satisfies $\theta_i\vec{k} = \vec{k} - \vec{G}'$ for a given reciprocal lattice vector $\vec{G}'$ ($\vec{G}' = 0$ when the *k* point is inside the first Brillouin zone). In the above expression, we introduce the irreducible ray representation whose character is given by:

$$\acute{\chi}^{\alpha}(R_i) = \chi^{\alpha}(R_i) e^{(i\vec{k}\bullet\vec{\tau}_i)} \tag{3.5}$$

This irreducible ray representation in most of the cases corresponds to those of the conventional irreducible representations of the point groups used in the analysis of molecules and thus we use the Mulliken symbols to express the representations. [48, 49] However, in some exceptional cases, the irreducible ray representations do not correspond to conventional irreducible representations as mentioned in the next paragraph. We implemented the above algorithm in the first-principles calculation code PHASE/0.[50]

3.2 Doubly Degeneracy on The First Brillouin Zone Edge.

We found that the degeneracy it caused by two reasons. First, the doubly degeneracy it caused by sticking of two-dimensional irreducible representation. Second, the degeneracy it caused by pairing of one-dimensional irreducible representation.

3.2.1 Degeneracy Induced by Sticking Two-Dimensional Irreducible Representation

In some cases of non-symmorphic systems, the sticking of bands occurs on the first Brillouin zone edge, i.e., only two-dimensional irreducible ray

representations are allowed on the zone boundary and their characters are different from those of the Mulliken ones. We clarify that all the bands are doubly degenerated on the zone edge (Fig.5.1). Here, we discuss the degeneracy on the S-C-Y line where the k group has the symmetry of C_{2v} (Table V.2) and symmetry operations $\{C_2(x)|\vec{\tau}\}$ and $\{\sigma_{xy}|\vec{\tau}\}$ include the fractional translation $\vec{\tau} = \frac{1}{2}\vec{a} + \frac{1}{2}\vec{b}$, where $\vec{a}$ and $\vec{b}$ are primitive lattice vectors in the x and y directions, respectively. When $e^{\{i(\theta_i - \vec{k})\cdot\vec{\tau}_i\}} \neq 1$ for an operation $\{\theta_i, \vec{\tau}_i\}$, the wavefunctions do not belong to the conventional irreducible representation.[50, 51] We find that $D = e^{\{i(C_2(x) - \vec{k})\cdot\vec{\tau}\}} = -1$ (Table V.2) and therefore the wavefunctions do not belong to conventional irreducible representation. Here we denote the irreducible representation using Γ_1.

3.2.2 Degeneracy Induced by Pairing of One-Dimentional Irreducible Representation.

Another type of doubly degeneracy is induced by time-reversal symmetry, which can be checked by calculating the Herring sum.[51]

$$S = \sum_m \chi^{\alpha}(Q_m^2) = \begin{cases} p\ (case\ a) \\ 0\ (case\ b) \end{cases} \tag{3.6}$$

where Q_m is a time-reversal symmetry operation which transforms $\vec{k}$ to $(-\vec{k} + \vec{G}_m)$ for a given reciprocal lattice vector $\vec{G}_m$ and p is the number of time-reversal symmetry operation. In the case of *b*, two levels belonging to different irreducible representations have the same energy.[52] On the other hand, this pairing does not occur in the case of *a*. We implemented the method above in PHASE/0, [53] so we are doing the identification of representations using computer.

Chapter 4

Geometry Structure of Group IV-VI Monolayers

4.1 Optimize Structure of Monolayer Group IV-VI Monolayer Materials.

Since the system form buckled puckered structure, the two top atoms are placed in different planes, and they have buckling height (*h*). We found that there were two cases, case I is namely positive buckling height and case II is negative buckling height. We define the buckling height (*h)* which is positive when the VI atoms are located at the lower positions (Fig. 1c and 1d) as figured in the following figure:

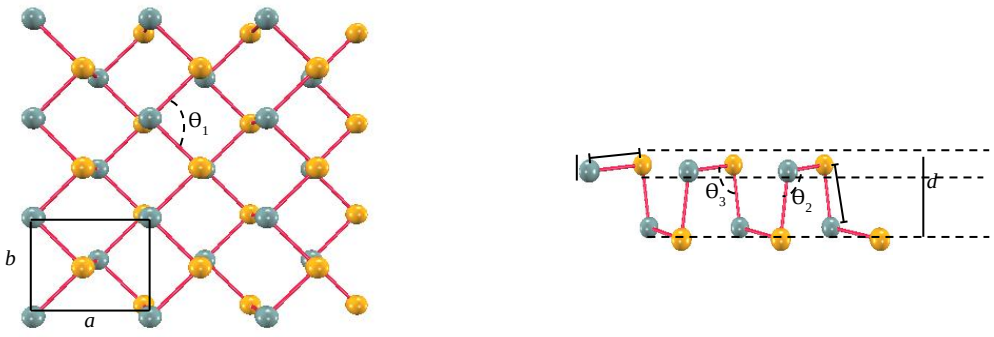

(a) (b)

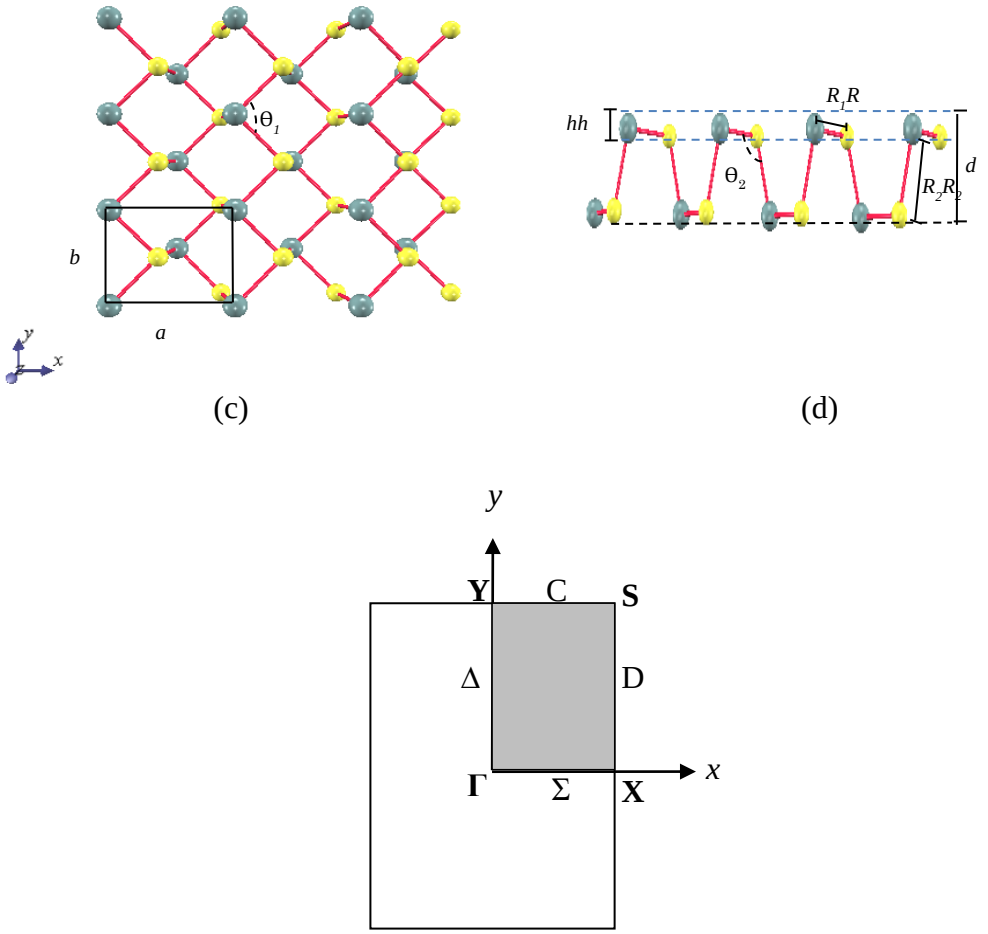

Fig. 4.1 (Color line) Top (a (c)) and side (b(d)) views of the buckled puckered structure n (negative (positive)) buckling height and the first Brillouin zone (e). Blue and yellow balls represent group IV and group VI atoms, respectively.

Meanwhile, the buckling amplitude (*h)* is negative when the VI atoms are located at the higher positions (Fig. 1a and 1b). For discuss what the reason of this buckling height, we calculate the electron density of GeS and GeSe monolayer for positive and negative buckling high respectively.

We first optimize the lattice constants and internal coordinates of the atoms (Table IV.1). We find that the two top atoms are buckled in the optimized structures (Fig.4.1) and thus systems belong to the space group $Pmn2_1(C_{2v}^7)$ as

well as the group V buckled puckered systems.[16] Since this space group is non-symmorphic, some symmetry operations have fractional translations as discussed later. Table IV.1 shows optimized structural parameters, which are close to previous calculational and experimental values.[17, 18, 28,5 4]

Table IV.1 Calculated structural parameters (a, b, R_1, R_2 and d) which are defined in Fig. 4. 1.

AB	a (Å)	b (Å)	R_1 (Å)	R_2 (Å)	d (Å)
CSe	4.07	3.03	1.96	2.01	1.84
CTe	4.36	4.25	2.16	2.18	2.08
SiO	4.53	2.68	1.83	1.83	1.31
SiS	4.82	3.33	2.26	2.33	2.17
SiSe	4.69	3.67	2.50	2.47	2.38
SiTe	4.36	4.25	2.62	2.76	2.72
GeO	4.45	3.06	1.99	2.00	2.00
GeS	4.67	3.61	2.44	2.44	2.35
GeSe	4.33	3.95	2.55	2.66	2.53
GeTe	4.36	4.25	2.73	2.88	2.72

4.2 Buckling Mechanism and Electron Transferred

We define the buckling amplitude (*h)* which is positive when the group VI atoms are located at the lower positions (Fig.4.1). We find that as the difference in the electronegativity ξ_B-ξ_A becomes large, h tends to increase (Fig. 4.2 and Table IV.2), where ξ_A and ξ_B are the electronegativities of the group IV and VI atoms, respectively. When ξ_B-ξ_A is sufficiently large (SiO, SiS, SiSe, GeO and GeS), i.e., ξ_B-ξ_A > 0.54, the VI atoms are located at the lower positions and thus h is positive. We find that as the IV atoms has smaller bond angle if we compare to the VI atoms. The IV atoms tend to form p^3 (90^0) orbital and the VI atoms tend to form sp^3 (120^0) orbitals. The IV atoms have smaller bond angle than the VI atoms. In addition, the VI atoms includes s orbital and thus their orbitals are energetically

stabilized as a consequence of large s component. Because of all this mechanism, we clarify the electron substantially transferred from higher position (the IV atoms) to the lower position (the VI atoms).

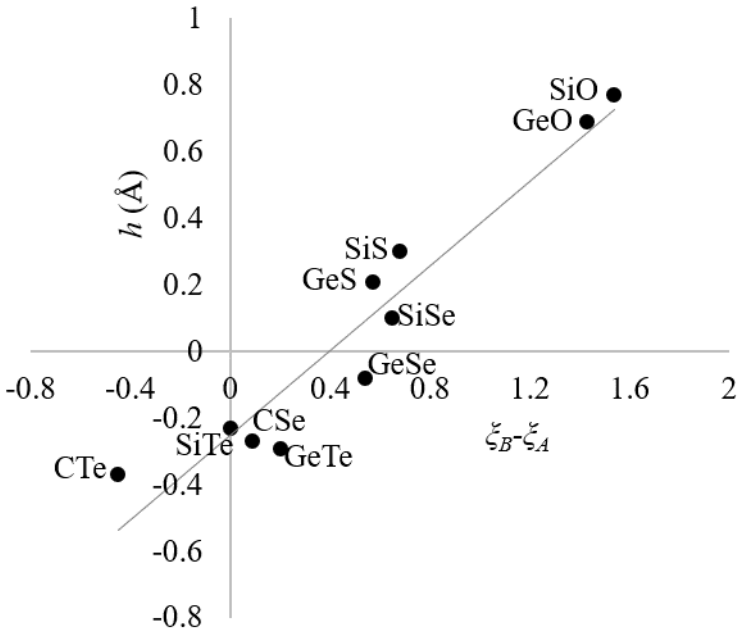

Fig. 4.2 Relationship between the buckling height, *h*, and the difference of electronegativities, ξ_B-ξ_A.

On the contrary, when ξ_B-ξ_A is negative (CTe), the VI atoms are located at the higher positions and *h* is negative. We also find that *h* is negative when ξ_B-ξ_A is positively small (CSe, SiTe, GeSe and GeTe), i.e., $0 < \xi_B$-$\xi_A < 0.54$. The group VI has smaller bond angle than the IV atoms. The VI atoms tend to form p^3 (90^0) orbital and group IV tend to form sp^3 (120^0) orbitals. Since the IV atoms includes s orbital and thus their orbitals are energetically stabilized as a consequence of large s component. In this case, the electron transferred is reduced. The VI atoms are favored located on the higher position and group IV on the lower position.

Table IV.2 Geometrical parameters and the difference of the electronegativities, ξ_B-ξ_A, which are determined by the Pauling scale.[17] The buckling amplitude, h, and the bond angles, θ_2 and θ_3, are defined in Fig. 4. 1.

	$\boldsymbol{\theta_2}$	$\boldsymbol{\theta_3}$	$\boldsymbol{\theta_3 - \theta_2}$	$\boldsymbol{h}$	$\boldsymbol{\xi_B - \xi_A}$
CSe	110.9	98.2	-12.7	-0.23	0.00
CTe	109.3	90.1	-19.2	-0.37	-0.45
SiO	94.2	132.5	38.3	0.77	1.54
SiS	96.3	111.1	14.8	0.3	0.68
SiSe	97.0	101.5	4.5	0.1	0.65
SiTe	100.3	87.8	-12.5	-0.29	0.20
GeO	91.3	126.5	35.2	0.69	1.43
GeS	94.9	106.2	11.3	0.21	0.57
GeSe	96.8	92.4	-4.4	-0.08	0.54
GeTe	99.9	87.3	-12.6	-0.27	0.09

Here we discuss the reason why the group VI atoms are located at the lower positions when ξ_B-ξ_A is large. Electrons substantially transfer from the IV atom to VI atom when ξ_B-ξ_A is large. In this case, the VI atoms are expected to be located at the lower positions because as Table IV.2 shows, the lower position atoms have larger bond angles and thus their orbitals are energetically stabilized as a consequence of large s component. As discussed in a previous paper,[14,16,17] this electron transfer from the higher position atom to the lower position atom also occurs even when the two atoms are of the same kind; This type of electrons transfer occurs in the case of the buckled puckered structure of group V two-dimensional systems.[14]

To check the validity of the above argument, we take GeS as an example and calculate the electron density for the valence band top (VBT) and conduction band bottom (CBB) (Fig. 4.3). The electronegativity of S is sufficiently larger than that of Ge (ξ_B-ξ_A = 0.57) and the Ge and S atoms are located at the higher and the lower positions, respectively. As Fig. 3.1 shows,

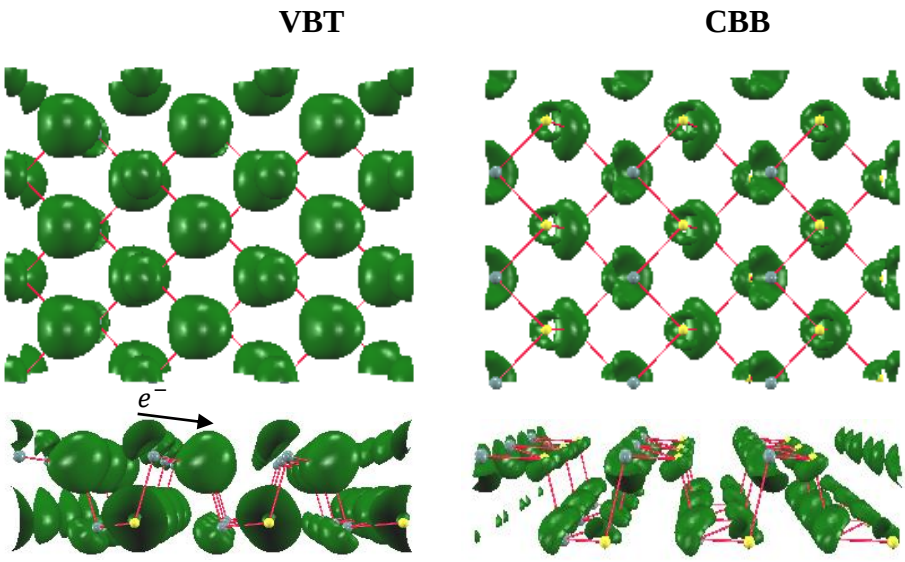

Fig. 4.3 (Color online) Electron density for the VBT (left-hand side) and CBB (right-hand side) of GeS. We integrate the electron densities over the energy width of 0.2 eV to the VBT (a) and from the CBB (b).

VBT and CBB mainly consist of S and Ge orbitals, respectively, which indicates that electrons transfer from Ge to S. Since the bond angle of S is larger than that of Ge, the orbitals of S tend to form sp^3 like orbitals (106.2^0) and Ge tend to form p^3 like orbitals (94.9^0). Since the s orbitals is including in Sulfur atom so the orbital energetically stable and has lower energy if compared to the Germanium atom, and Sulfur atom is located is located in lower position (Fig. 4.1).

Next, we discuss the reason why the IV atoms are located at the lower positions when the absolute value ξ_B-ξ_A is small i.e CSe, CTe, SiTe, GeSe and GeTe monolayers materials. We take CTe as an example and calculate the electron density for the valence band top (VBT) and conduction band bottom (CBB) (Fig. 4. 4). The electronegativity of Te is sufficiently lower than that of C (ξ_B-ξ_A = -0.45), the C atom favored located at the lower position and has bigger bond angle meanwhile then the Te atoms are favored located at the higher positions and has lower bond angle as Fig. 4.4 shows. In contrast to positive buckling height, in this case the electron transferred is small or there is no electron transferred.

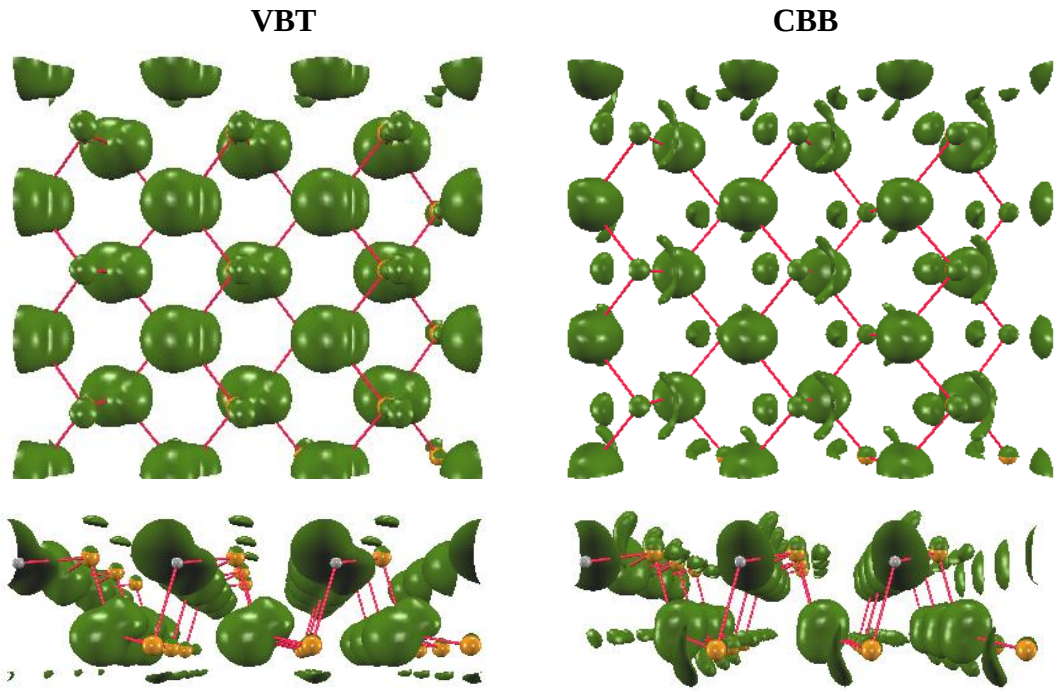

Fig. 4.4 (Color online) Electron density for the VBT (left-hand side) and CBB (right-hand side) of GeSe. We integrate the electron densities over the energy width of 0.2 eV to the VBT (a) and from the CBB (b).

VBT and CBB mainly consist of C and Te orbitals, respectively. Since the bond angle of C is larger than that of Te, the orbitals of C tend to form sp^3 like orbitals (109.3) and Te tend to form p^3 like orbitals (90.1). Since the s orbitals is including in C atom so the orbital energetically stable and has lower energy than Te atom.

Chapter 5

Band Structures of the Monolayer Analyzed Based on the Group Theory

In this chapter we discuss the analysis of band structure based on the group theory. We calculate the band structures of the monolayer systems. In most parts of the Brillouin zone, wavefunctions belong to conventional irreducible representations. In this case, we use Mulliken symbols in Fig. 5.1.[45, 46] In the other cases, we use the numerical notations.

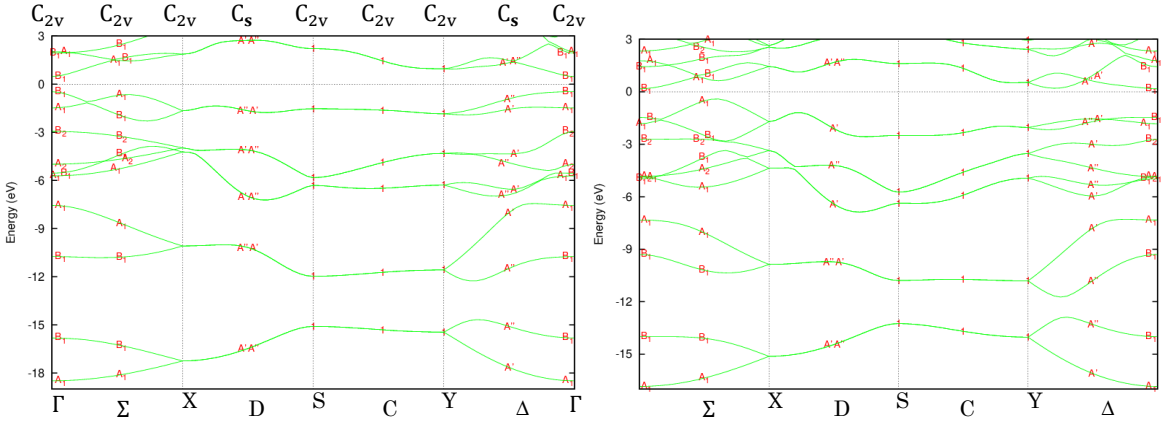

(a) CSe (b) CTe

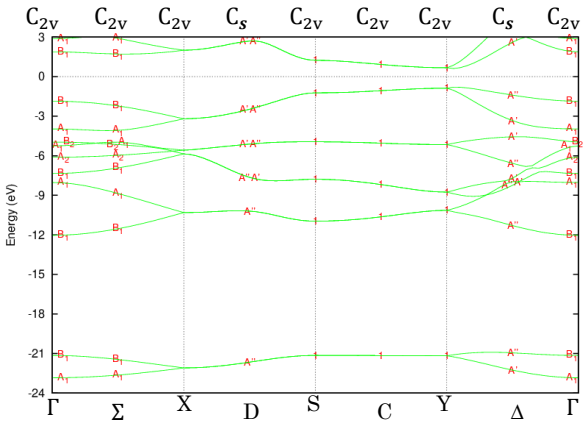

(c) SiO

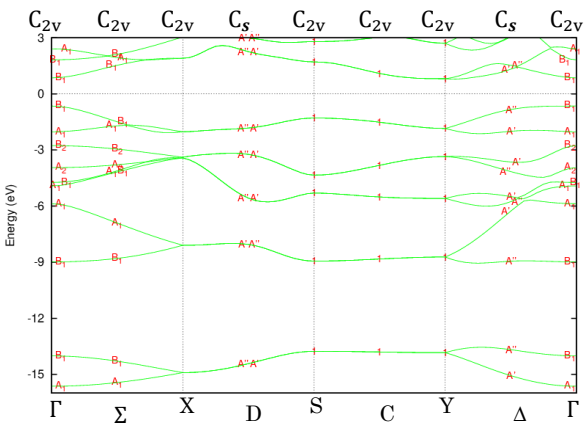

(d) SiS

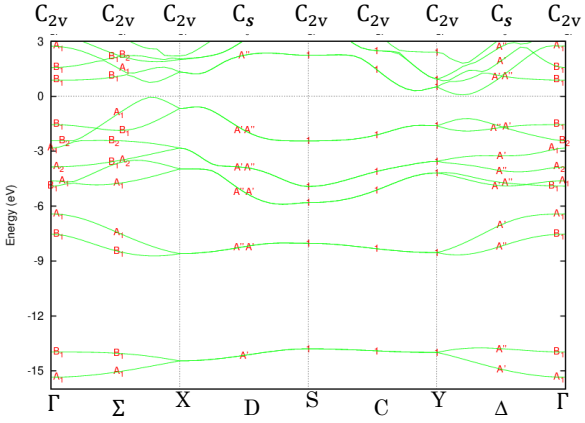

(e) SiSe

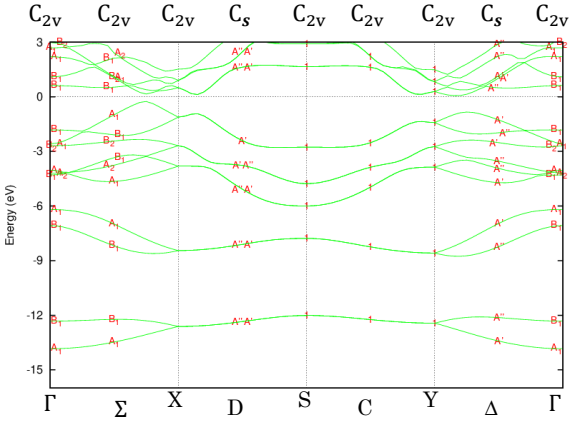

(f) SiTe

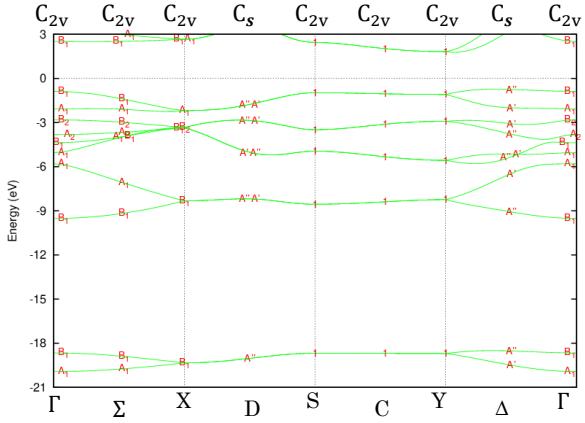

(g) GeO

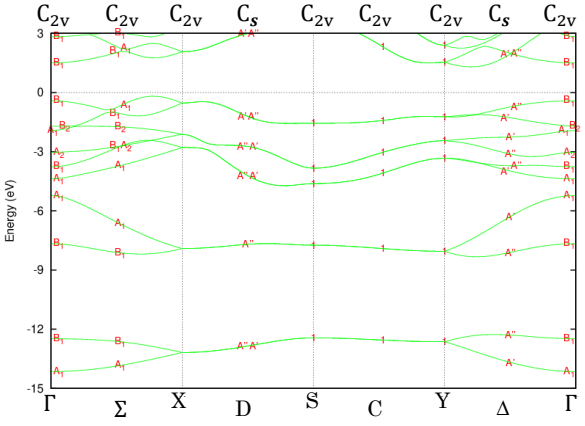

(h) GeS

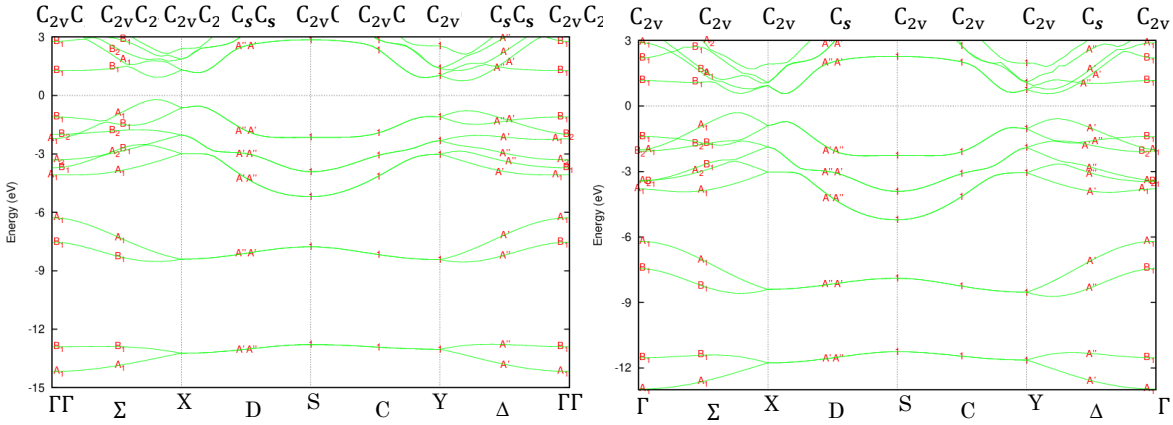

(i) GeSe (j) GeTe

Fig. 5. 1 (Color online) Band structures of buckled puckered structures of (a) CSe (b) CTe (c) SiO (d) SiS (e) SiSe (f) SiTe (g) GeO (h) GeS (i) GeSe (j) GeTe. We use Mulliken symbols for one-dimensional irreducible representations (A_1,A_2,B_1,B_2) for Γ, Σ, X line and A', A'' for D line. We denote Γ_1 by 1 on the S-C-Y line in the figures.

We clarify that all the bands are doubly degenerated on the zone edge (5. 1). First, we discuss the degeneracy on the S-C-Y line where the k group has the symmetry of C_{2v} (Table V.2) and symmetry operations $\{C_2(x)|\vec{\tau}\}$ and $\{\sigma_{xy}|\vec{\tau}\}$ include the fractional translation $\vec{\tau} = \frac{1}{2}\vec{a} + \frac{1}{2}\vec{b}$, where $\vec{a}$ and $\vec{b}$ are primitive lattice vectors in the x and y directions, respectively. When $e^{\{i(\theta_i - \vec{k})\cdot\vec{\tau}_i\}} \neq 1$ for an operation $\{\theta_i, \vec{\tau}_i\}$, the wavefunctions do not belong to the conventional irreducible representation. [56] We find that $D = e^{\{i(C_2(x) - \vec{k})\cdot\vec{\tau}\}} = -1$ (Table V. 2) and therefore the wavefunctions do not belong to conventional irreducible representations; only one irreducible ray representation Γ_1 whose characters are shown in Table V.1 is allowed. Since Γ_1 is two-dimensional, the sticking of bands occurs on the S-C-Y line, i. e., all the bands are doubly degenerated.

Table V.1 Character table for *k* groups.

	Irreducible Representation	E	$C_2(x)$	σ_{xz}	σ_{xy}
$X(C_{2v})$	A_1	1	1	1	1
	A_2	1	1	-1	-1
	B_1	1	-1	1	-1
	B_2	1	-1	-1	1
$S(C_{2v})$	Γ_1	2	0	0	0
$C(C_{2v})$	Γ_1	2	0	0	0
$Y(C_{2v})$	Γ_1	2	0	0	0
$D(C_s)$	A'	1			1
	A''	1			-1

Table V.2 Group theoretical analysis for some *k* points.

***k* point**	**Point Group**	**Symmetry operation**	***D***	**Irreducible Representation**	**Time-reversal element**	**Herring Sum**	**Pairing**
Γ	C_{2v}	$\{E\|0\}$ $\{C_2(x)\|\vec{\tau}\}$ $\{\sigma_{xz}\|0\}$ $\{\sigma_{xy}\|\vec{\tau}\}$	1	$A_1, \mathrm{B}_1, \mathrm{A}_2, \mathrm{B}_2$	$\{E\|0\}$ $\{C_2(x)\|\vec{\tau}\}$ $\{\sigma_{xz}\|0\}$ $\{\sigma_{xy}\|\vec{\tau}\}$	4	No pairing
Σ	C_{2v}	$\{E\|0\}$ $\{C_2(x)\|\vec{\tau}\}$ $\{\sigma_{xz}\|0\}$ $\{\sigma_{xy}\|\vec{\tau}\}$	1	$A_1, \mathrm{B}_1, \mathrm{A}_2, \mathrm{B}_2$	No time-reversal element	-	No pairing
X	C_{2v}	$\{E\|0\}$ $\{C_2(x)\|\vec{\tau}\}$ $\{\sigma_{xz}\|0\}$ $\{\sigma_{xy}\|\vec{\tau}\}$	1	$A_1, \mathrm{B}_1, \mathrm{A}_2, \mathrm{B}_2$	$\{E\|0\}$ $\{C_2(x)\|\vec{\tau}\}$ $\{\sigma_{xz}\|0\}$ $\{\sigma_{xy}\|\vec{\tau}\}$	0	(A_1, B_1) (A_2, B_2)
D	C_s	$\{C_2(x)\|\vec{\tau}\}$ $\{\sigma_{xy}\|\vec{\tau}\}$	1	A', A''	$\{C_2(x)\|\vec{\tau}\}$ $\{\sigma_{xy}\|\vec{\tau}\}$	0	(A', A'')

$\boldsymbol{S}$	$\boldsymbol{C_{2v}}$	$\{E\|0\}$ $\{C_2(x)\|\vec{\tau}\}$ $\{\sigma_{xz}\|0\}$ $\{\sigma_{xy}\|\vec{\tau}\}$	-1	Γ_1	$\{E\|0\}$ $\{C_2(x)\|\vec{\tau}\}$ $\{\sigma_{xz}\|0\}$ $\{\sigma_{xy}\|\vec{\tau}\}$	4	No pairing
$\boldsymbol{C}$	$\boldsymbol{C_{2v}}$	$\{E\|0\}$ $\{C_2(x)\|\vec{\tau}\}$ $\{\sigma_{xz}\|0\}$ $\{\sigma_{xy}\|\vec{\tau}\}$	-1	Γ_1	No time-reversal element	-	No pairing
$\boldsymbol{Y}$	$\boldsymbol{C_{2v}}$	$\{E\|0\}$ $\{C_2(x)\|\vec{\tau}\}$ $\{\sigma_{xz}\|0\}$ $\{\sigma_{xy}\|\vec{\tau}\}$	-1	Γ_1	$\{E\|0\}$ $\{C_2(x)\|\vec{\tau}\}$ $\{\sigma_{xz}\|0\}$ $\{\sigma_{xy}\|\vec{\tau}\}$	4	No pairing
Δ	$\boldsymbol{C_s}$	$\{C_2(x)\|\vec{\tau}\}$ $\{\sigma_{xy}\|\vec{\tau}\}$	1	A', A''	$\{C_2(x)\|\vec{\tau}\}$ $\{\sigma_{xy}\|\vec{\tau}\}$	2	No pairing

On the other hand, on the X-D line, the wavefunctions belong to conventional irreducible representations denoted by Mulliken symbols because of *D=1*. We find that all the bands belong to a one-dimensional representation since the symmetry is not high (C_{2v} and C_s) as Fig. 5.1 shows. However, we find that all the bands are paired because of the time-reversal symmetry. We evaluate the Herring sum in Eq. (6) and find that the sum equals to 0, indicating that two different irreducible representations are paired (Table V.2). As Table V.2 shows, A_1 and B_1 (A_2 and B_2) are paired at the X point where the symmetry is C_{2v}. A' and A'' are paired on the D line where the symmetry is C_s.

Based on the argument mentioned above, we conclude that the degeneracy on the first Brillouin zone edge is due to the symmetry of this system. The degeneracy on the S-C-Y line occurs due to the sticking of the bands on the first Brillouin zone edge. Meanwhile, for the X-D line, the degeneracy is caused by the time-reversal symmetry. The above-mentioned degeneracy on the Brillouin zone edge is expected to be detected by some experiments such as photoelectron

spectroscopy. This degenerated bands may split when we include the spin-orbit coupling. [55]

Chapter 6

Summary and Future Works

6.1 Conclusions

We have carried out first-principles calculations of group IV-VI two-dimensional monolayer materials. The systems form buckled geometries and thus the space group is $Pmn2_1(C_{2v}^7)$ that belong to non-symmorphic group. We conclude that when the electronegativity difference $(\xi_B\text{-}\xi_A)$ is large, the group VI atoms are located at the lower positions. The VI atoms are expected to be located at the lower positions because VI atoms have larger bond angles and thus their orbitals are energetically stabilized as a consequence of large s component. On the contrary, if the difference is positively small or negative, group VI atom is located at the higher positions.

We use Mulliken symbols to denote the irreducible representation. When $e^{\{i(\theta_i-\vec{k})\bullet\vec{\tau}_i\}} \neq 1$ for an operation $\{\theta_i, \vec{\tau}_i\}$, the wavefunctions do not belong to irreducible representation. In some cases, we use the numerical notations, Γ_1, caused $D = e^{\{i(C_2(x)-\vec{k})\bullet\vec{\tau}\}} = -1$. We find that all the bands are doubly degenerated on the first Brillouin zone edge. We clarify that this degeneracy is due to the symmetry of this system. The degeneracy on the S-C-Y line occurs due to the sticking of the bands on the first Brillouin zone edge. Meanwhile, for the X-D line degeneracy caused by the time-reversal symmetry.

6.2 Future Scope

We have studied the buckling mechanism and the degeneracy on the first Brillouin zone of group IV-VI two-dimensional monolayer materials based on density functional theory. We have found that the buckling height occurs caused the different of electronegativity. When the electronegativity differences large, the

buckling height is positives and the electron substantially transfer from IV atoms to VI atoms. In contrary, when the buckling height become smaller, the electron transfer is reduced. We find that all the bands are doubly degenerated on the first Brillouin zone edge. We clarify that this degeneracy is due to the symmetry of this system. We find degeneracies on the whole or a part of first Brillouin zone edges and this degeneracy is analyzed based on the group theory. The degeneracies originate from pairing of conventional one-dimensional irreducible representation or from nonconventional two-dimensional irreducible representation. In the future research we can calculate the electronic structure of bilayer group IV-VI two dimensional materials.

References

1) K. S. Novoselov, A. K. Geim, Morozov, S. V. Jiang, D. Zhang, Y. Dubonos, S. V. Grigorieva and A. A. Firsov, Sci. 9, 306666 (2004).
2) G. Eda, G. Fanchini, and M. Chhowalla, Nanotech. 3, 270, 4 (2008).
3) S. Cahangirov, M. Topsakal, E. Akturk, H. Sahin, and S. Ciraci, Phys. Rev. Lett. 102, 236804 (2009).
4) P. Vogt, P. D. Padova, S. Quaresima, J. Avila, E. Frantzeskakis, M. C. Asensio, A. Resta, B. Ealet, and G. L. Lay, Phys. Rev. Lett. 108, 155501 (2012).
5) S. Huang, W. Kang, and L. Yang, Appl. Phys. Lett. 102, 133106 (2013).
6) E. Blanco, S. Butler, S. Jiang, O. D. Restrepo, W. Windi, and J. E. Goldberger, ACS Nano 7, 4414 (2013).
7) F. Zhu, W. Chen, Y. Xu, C. Gao, D. Guan, D. Qian, S. Zhang, and J. Jia, Nat. Mater. 14, 1020 (2015).
8) B. Liu, K. Zhou, Recent Progress on Graphene-analogous 2D Nanomaterials: Properties, Modeling and Applications, Progress in Materials Science (2019).
9) H. Sahin, S. Cahangirov, M. Topsakal, E. Bekaroglu, E. Akturk, R. T. Senger, and S. Ciraci, Phys. Rev. B80, 155453 (2009).
10) L. Li, Y. Yu, G. Ye, J. Q. Ge, X. Ou, H. Wu, D. Feng, X. H. Chen, and Y. Zhang, Nat. Nanotechnol. 9, 372 (2014).
11) H. Liu, A. T. Neal, Z. Zhu, Z. Luo, X. F. Xu, D. Tomanek and P. D. Ye, ACS Nano. 8, 4033(2014).
12) E. S. Reich, Sci Nat. 19, 506(2014).
13) T. Hong, B. Chamlagain, W. Lin, H. J. Chuang, M. Pan, Z. Zhou, and Y. Q. Xu, Nanoscale 6, 8978 (2014).
14) A. P. N. Nuning and M. Saito, Jpn. J. Appl. Phys. 58, 061003 (2019).
15) Qiao, J. S., Kong, X. H., Hu, Z., Yang, F and Ji, W., Nat. Commun. 5, 4475(2014).
16) M. Saito, Y. Takemori, T. Hashi, T. Nagao, and S. Yaginuma, Jpn. J. Appl. Phys. 46, 7824 (2007).
17) C. Kamal and M. Ezawa, Phys. Rev. B 91, 085423 (2016).

18) Y. Xu, B. Peng, H. Zhang, H. Shao, R. Zhang, and H. Zhu, Ann. Phys. (Berlin) 529, 1600152 (2017).
19) M. Pumera and Z. Sofer, Adv. Mater. 29, 1605299 (2017).
20) S. Sharma, S. Kumar, and U. Schwingenschlögl, Phys. Rev. Appl. 8, 044013 (2017).
21) O. U. Akturk, V. O. Ozcelik, and S. Ciraci, Phys. Rev. B 91, 235446 (2015).
22) M. F. Deschênes, O. Waller, T. O. Menteş, A. Locatelli, S. Mukherjee, F. Genuzio, P. L. Levesque, A. Hébert, R. Martel, and O. Moutanabbir, Nano Lett. 17, 4970 (2017).
23) P. Ares, J. J. Palacios, G. Abellán, J. G. Herrero, and F. Zamora, Adv. Mater. 30, 1703771 (2017).
24) E. Akturk, O. U. Akturk, and S. Ciraci, Phys. Rev. B 94, 014115 (2016).
25) M. Y. Liu, Y. Huang, Q. Y. Chen, Z. Y. Li, C. Cao, and Y. He, RSC Adv. 7, 39546 (2017).
26) T. Nagao, J. T. Sadowski, M. Saito, S. Yaginuma, Y. Fujikawa, T. Kogure, T. Ohno, Y. Hasegawa, S. Hasegawa, and T. Sakurai, Phys. Rev. Lett. 93, 105501 (2004).
27) M. Saito, T. Ohno, and T. Miyazaki, Appl. Surf. Sci. 237, 80 (2004).
28) Hu, Z. Yingchun, D. Xuemin, H. Wenhan, Z. Xuechao, Y. and Shengli, Z. *Nanotechnology* 30, 252001(2019).
29) Y. Tanaka, M, Saito and F. Ishii., Jpn. J. Appl. Phys. 57, 125201(2018).
30) H. L. Zhuang, A. K. Singh and R. G. Hennig, Phys. Rev. B 87, 165415 (2013).
31) H. L. Zhuang and R. G. Hennig, Appl. Phys. Lett. 101, 153109 (2012).
32) B. R Tuttle, S. M. Alhassan and S. T. Pantelides, Phys. Rev. 92, 235405 (2016).
33) F. Li, X. H. Liu, Y. Wang and Y. F. Li, J. Mater. Chem. C 4, 2155 (2016).
34) B. R. Tuttle, S. M. Alhassan and S. T. Pantelides, Phys. Rev. 92, 235405 (2015).
35) S. L. Zhang, N. Wang, S. G. Liu, S. P. Huang, W. H. Zhou, B. Cai, M. Q. Xie, Q. Yang, X. P. Chen and H. B, Zeng, Nanotechnol, 27, 274001 (2016).
36) F. Tuomisto, V. Ranki, D. C. Look, and G. C. Farlow, Phys. Rev B, 76, 165207 (2007).
37) W. Kohn and L. J. Sham, Phy. Rev, 140, A1133 (1965).

38) Jorge Jos´e Kohanoff, *Electronic Structure Calculations for Solids and Molecules: Theory and Computational Methods*. Cambridge Univ. Press, Cambridge, 2006. ISBN 978-0-521-81591-8. OCLC: 254698805.
39) P. S. Svendsen and U. von Barth. Phy. Rev B, 54, 17402 (1996).
40) John P. Perdew Kieron Burke, J. Qua.Chem, p.309–319 (1996).
41) Hamann, M. Schl¨uter, and C. Chiang, Phys. Rev. Lett, 43, 1494 (1979).
42) D. Vanderbilt, Phys. Rev B, 41, 7892 (1990).
43) PHASE/0[https://azuma.nims.go.jp/cms1].
44) D. Vanderbilt, Phys. Rev. B 41, 7892 (1990).
45) D. R. Hamann, M. Schlüter, and C. Chiang, Phys. Rev. Lett. 43, 1494 (1979).
46) Y. Mao, C. Xu, J. Yuan, H Zhao, J. Chem. Soc, (2018).
47) V. Heine, *Group Theory in Quantum Mechanics* (Pergamon Press, London, 1960).
48) R. S. Mulliken, J. Chem. Phys. 23, 1997 (1955).
49) R. S. Mulliken, J. Chem. Phys. 24, 1118 (1956).
50) G. Burns, *in Introduction to Group Theory with Applications*, ed. A. M. Alper and A. S. Nowick (Academic, New York, 1977), p. 323.
51) M. S. Dresselhaus, G Dresselhaus, A. Jario, *Group Theory*. (Cambridge, MA, USA, 2008).
52) J. P. Perdew and Y. Wang, Phys. Rev. B 45, 13244 (1992).
53) J. P. Perdew, K. Burke, and M. Ernzerhof, Phys. Rev. Lett. 77, 3865 (1996).
54) L. Bolin, *Nonsymmorphic Symmetries and Their Consequences* (Massachusetts Institute of Technology, 2012).
55) S. D. Guo and Y. H. Wang, J. Appl. Phys. 121, 034302 (2017).

Appendix A

Optimized of Buckled-Puckered Structure Group IV-VI Two-Dimensional Monolayer Materials.

In Chapter 4, we mentioned the optimized structure of group IV-VI two-dimensional monolayers materials form the buckled-puckered structure. In the buckled-puckered structure, the two top atoms are placed in different plane, and they have buckling height (h). In this part, we figured out the different of positive and negative buckling height.

a. Positive Buckling Height

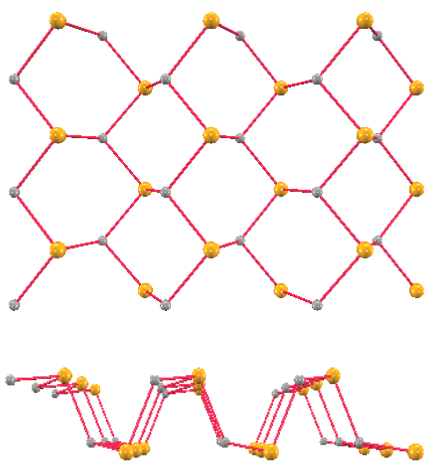

(a) CSe

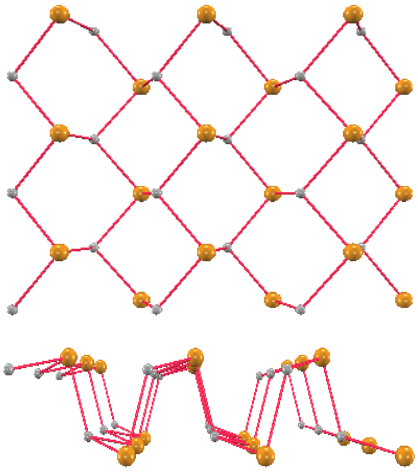

(b) CTe

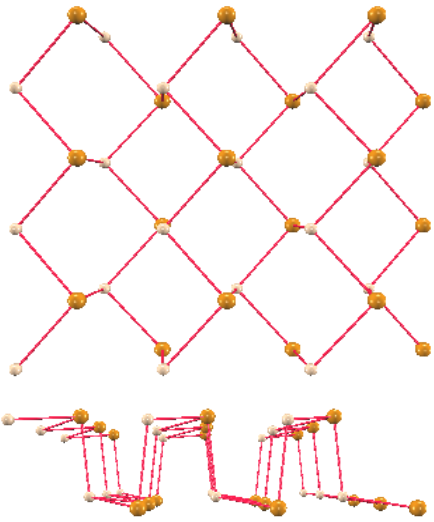

(c) SiTe

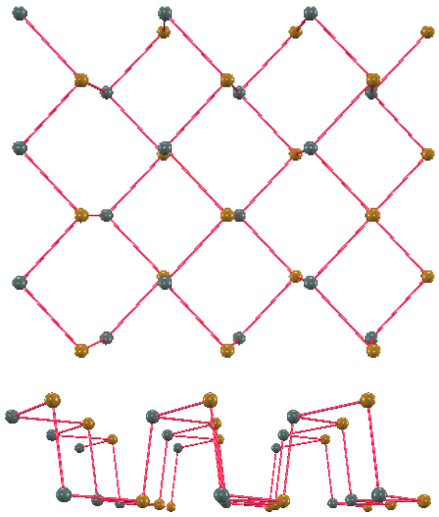

(d) GeSe

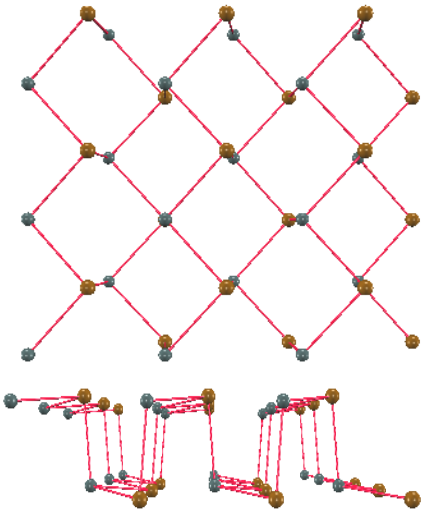

(e) GeTe

Fig.1 (Color line) Top and side views of the buckled puckered structure negative buckling height of CSe (a), CTe (b), SiTe (c) monolayer materials

b. **Negative Buckling Height**

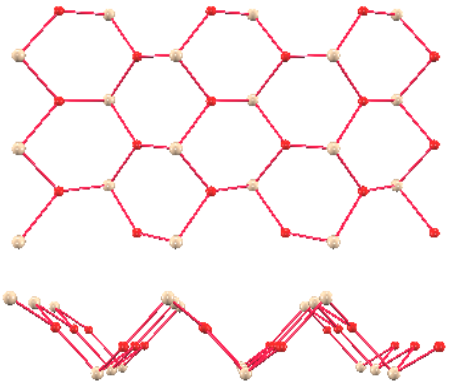

(a) SiO

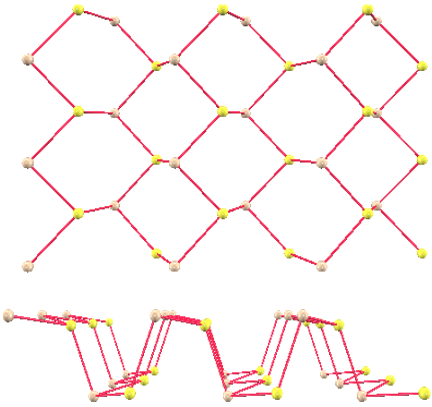

(b) SiS

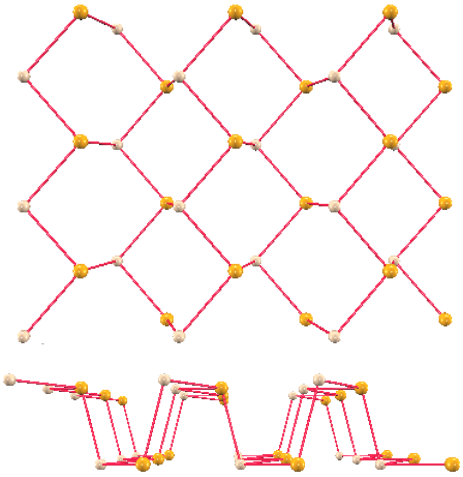

(c) SiSe

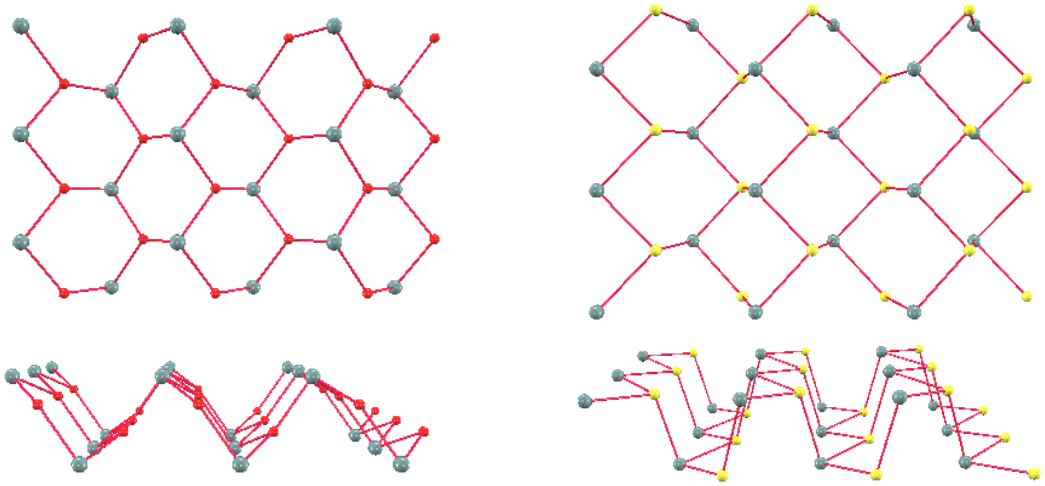

(d) GeO (e) GeS

Fig.2 (Color line) Top and side views of the buckled puckered structure positive buckling height of SiO(a), SiS(b), SiSe(c), GeO(d), GeS(e) monolayer materials

Appendix B

Electron Density Group IV-VI Two-Dimensional Monolayer Materials.

In the chapter. 4 we explain the reason of the buckling mechanism and the electron transferred. To check the validity of the above argument, we calculate the electron density for the valence band top (VBT) and conduction band bottom (CBB) of the monolayers.

a. Negative Buckling height

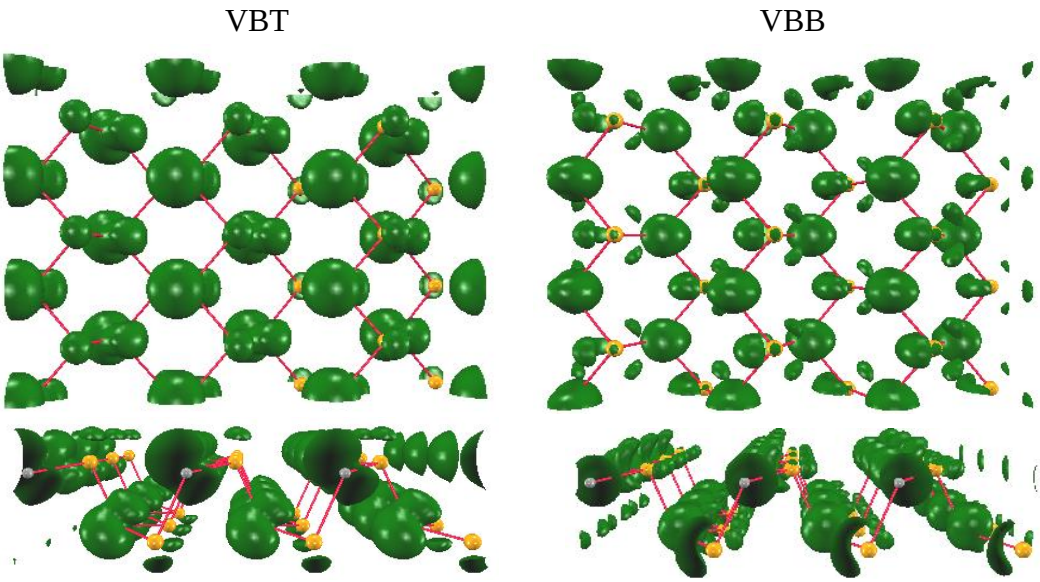

(a) CSe

VBT VBB

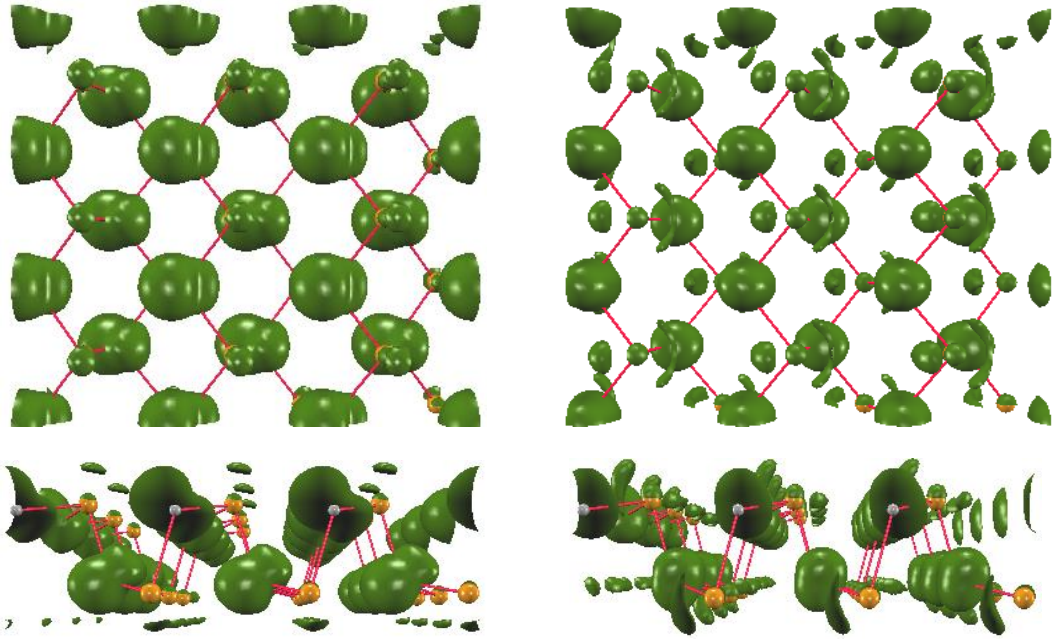

(b) CTe

VBT VBB

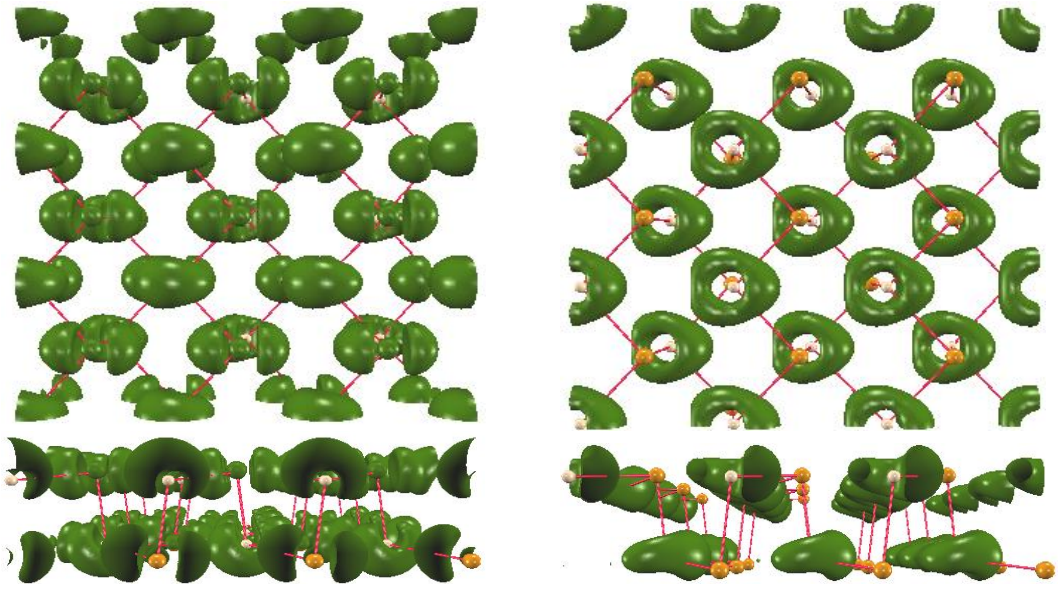

(c) SiTe

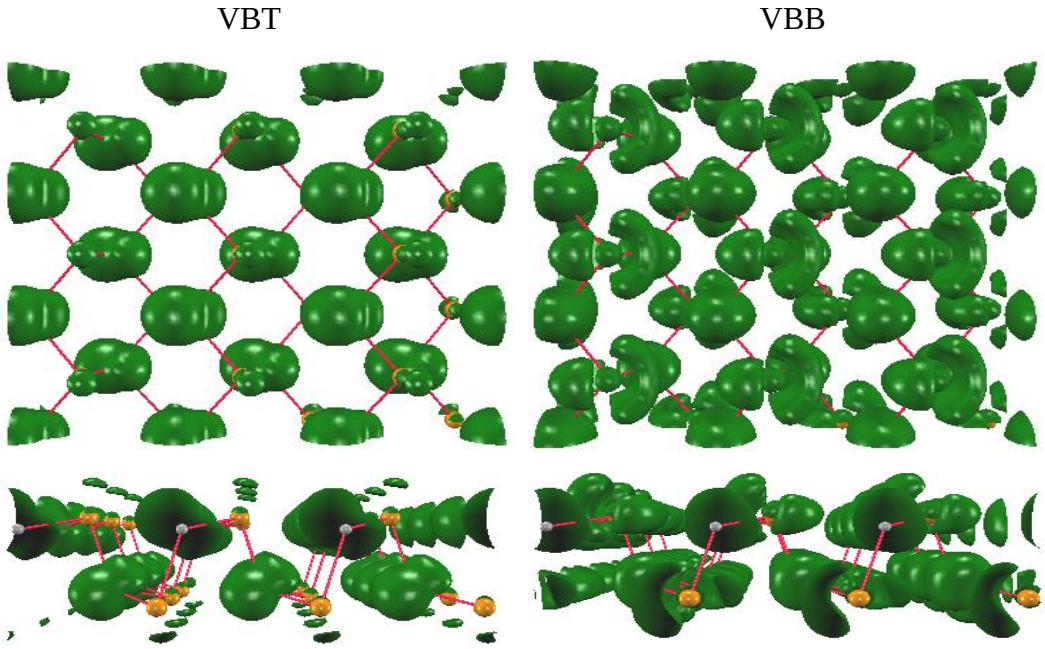

(d) GeSe

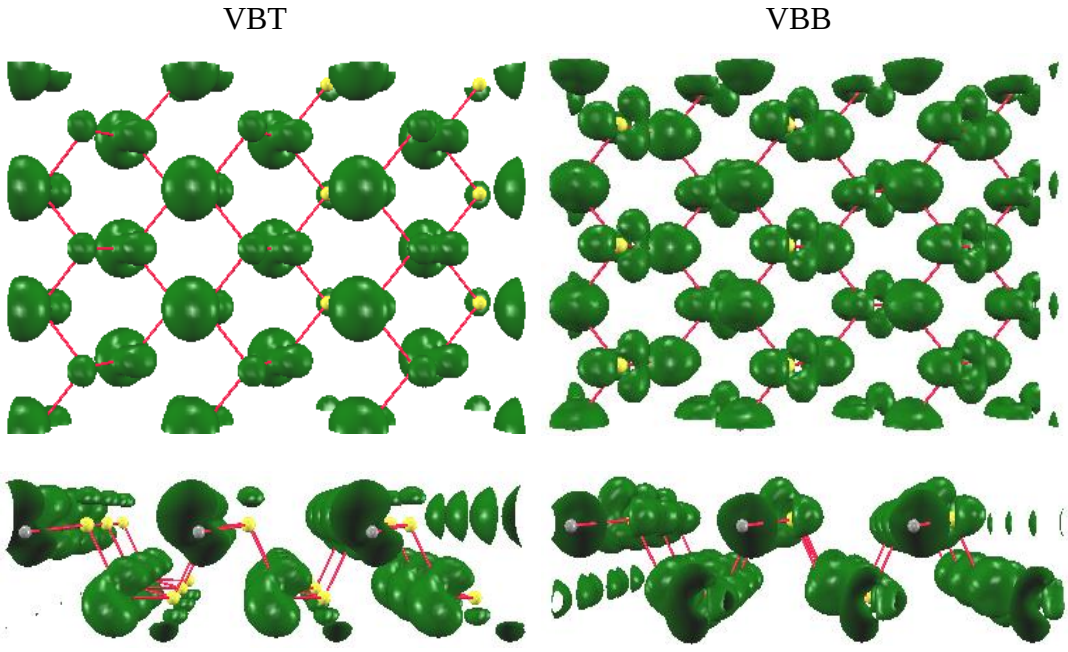

(e) GeTe

Fig. 1 Electron density for the VBT (left-hand side) and CBB (right-hand side) of group IV-VI two-dimensional monolayers materials. We integrate the electron densities over the energy width of 0.2 eV to the VBT (a) and from the CBB (b).

b. Positive Buckling Height

VBT VBB

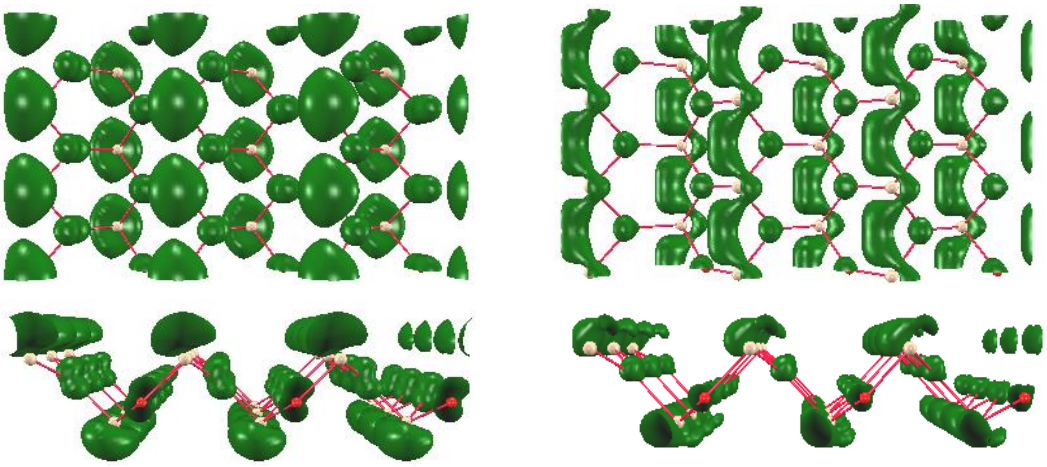

(a) SiO

VBT VBB

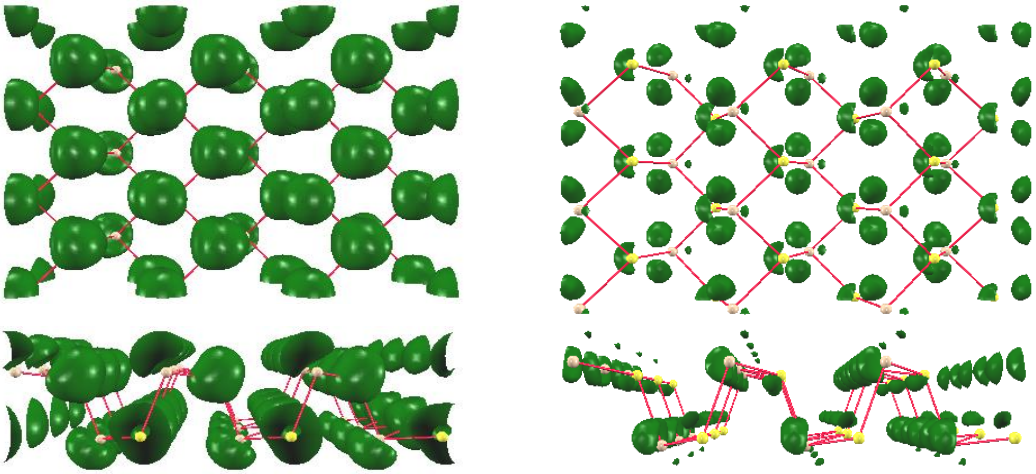

(b) SiS

VBT VBB

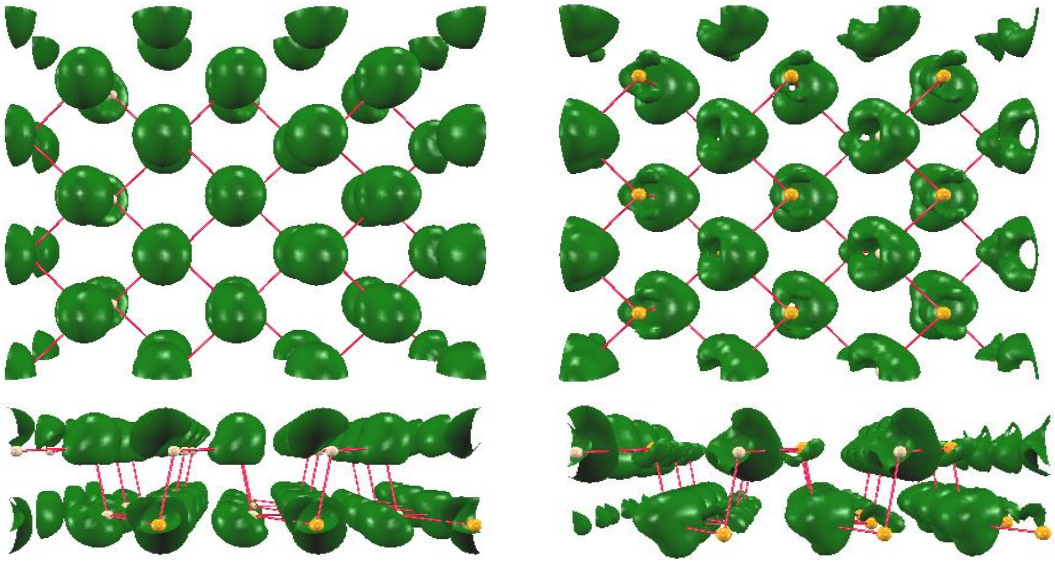

((c) SiSe

VBT VBB

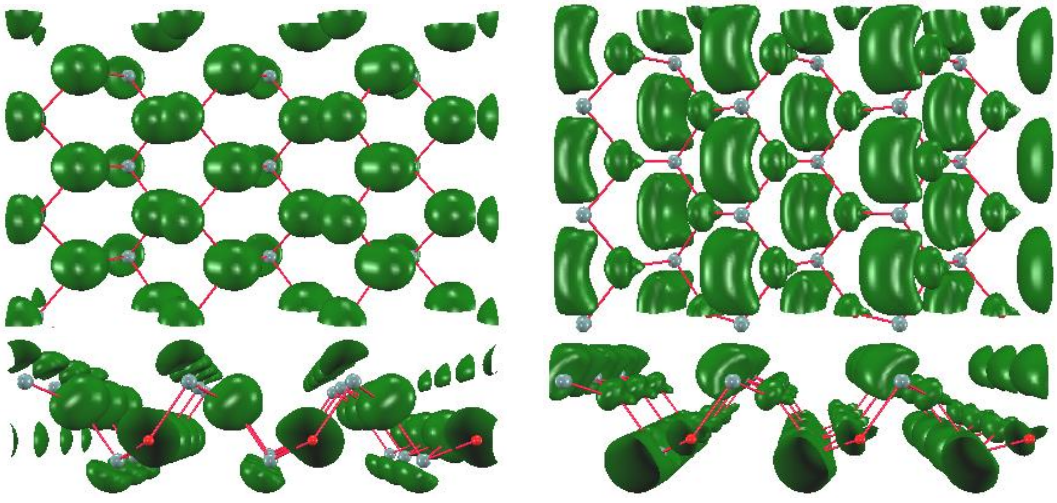

(d) GeO

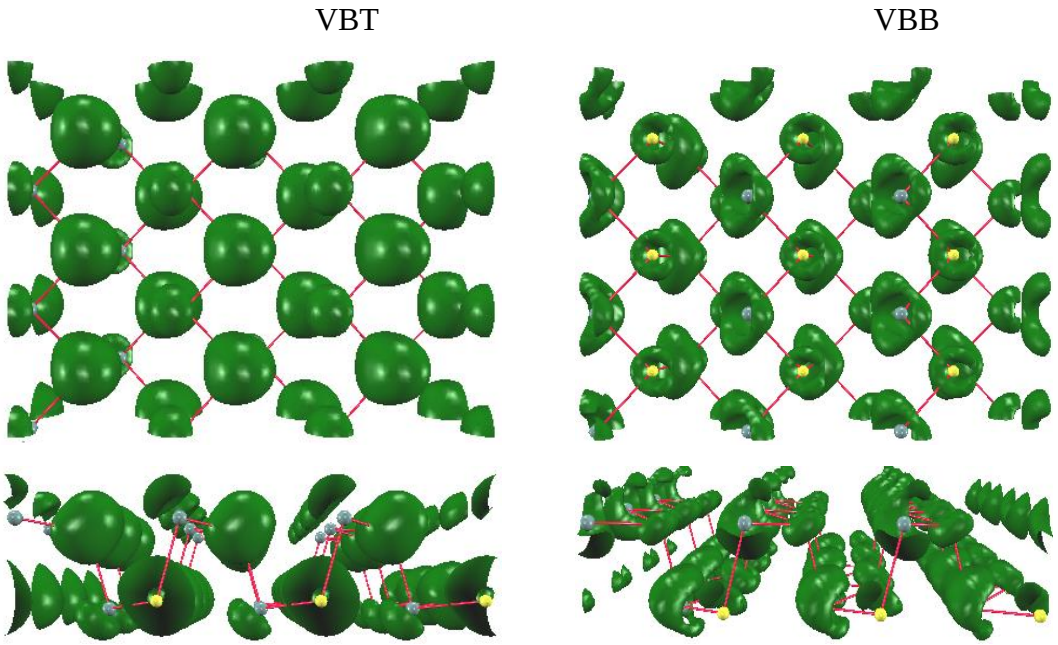

(e) GeS

Fig. 2 Electron density for the VBT (left-hand side) and CBB (right-hand side) of group IV-VI two-dimensional monolayers materials. We integrate the electron densities over the energy width of 0.2 eV to the VBT (a) and from the CBB (b).